CHAPTER 5

LASER-INDUCED BREAKDOWN SPECTROSCOPY EXPERIMENTATION AND APPLICATIONS

Zuhaib Haider[1], Kashif Tufail[2], Sufi Roslan[3], Yusof Munajat[2]

[1]Faculty of Applied Sciences and Technology (FAST),
Universiti Tun Hussein Onn Malaysia, Pagoh, 84600 Johor, Malaysia
[2]Physics Department, Faculty of Science, Universiti Teknologi Malaysia,
81310 Johor Bahru, Malaysia
[3]Center for Diploma Studies, Universiti Tun Hussein Onn Malaysia,
Pagoh, 84600 Johor, Malaysia

5.1 INTRODUCTION

This is an era of rapid production and fast growth. Reliable and fast analytical testing techniques are an essential part of manufacturing industries and testing and certifying authorities. Laser-Induced Breakdown Spectroscopy (LIBS) is one of the highly potential techniques to compete in this competitive arena for rapid elemental analysis which can be further used for real-time composition monitoring in the production line, post-production inspection, scrap sorting and even for classification of biological samples. In addition, remote and stand-off modes of operation increase the application potential of LIBS by many folds. It can be deployed in physically inaccessible or potentially unsafe areas. Compact LIBS systems have made its portability possible which implies ease of in-situ deployment.

LIBS can be used for qualitative and quantitative investigations. However, in general, quantitative analysis is not a strong point of LIBS as of now. It has been improved over the years for certain applications and still getting better as the researchers develop and refine the procedures for data collection and analysis.

To enhance an analytical technique, the understanding of underlying principles is crucial. Therefore, the continuity of research on fundamental aspects of a scientific method is significant unless fully understood. The research is ongoing, and innovative ways of utilising LIBS is of paramount importance for innovative applications with better reliability.

As experimental scientists working on LIBS technique, our task is to utilise experimental methodologies to understand the underlying principles governing LIBS and unlock its enormous potential.

There are two types of most common LIBS configurations which are Single-Pulse (SP) and Double-Pulse (DP) configurations [1] whereas double-pulse configuration has further variants. Also, there are two modes of quantitative measurements, i.e., Calibration and Calibration-Free (CF-LIBS). The ideal setup for LIBS would be a Single-Pulse Calibration Free LIBS. There have been significant achievements with CF-LIBS in recent years which lift our expectations to see it applied for real-world applications in near future.

Following sections provide a brief overview and compilation of some of the LIBS investigations performed by the author. It includes fundamental studies and application-based investigations.

5.2 Basic LIBS Setup

Basic LIBS setup is very simple; it only requires a laser, a spectrometer and some optical components to focus the laser beam onto the sample and collect radiation emissions from plasma. However, for experimental investigations in laboratory, we tend to include more paraphernalia to increase no. of aspects for exploratory investigations from various aspects. A typical laboratory LIBS setup is schematically illustrated in Fig. 5.1. It consists of a sample chamber to control the environment around the sample. Laser enters the sample chamber through a laser port (usually Quartz) and converges on to the sample surface by a focusing lens. For continuous monitoring, the energy delivered by the laser pulses, a beam splitter is placed in the beam path to reflect a fraction of laser beam to the energy meter. Emissions from laser-induced plasma are collected through collection port of the chamber and focussed into a fibre optic cable (FOC) which delivers these optical radiations to a spectrometer with minimal loss. The spectrometer splits these radiations into a spectrum of wavelengths and intensities and transfers the spectral data to a computer where it is conveniently stored and analysed.

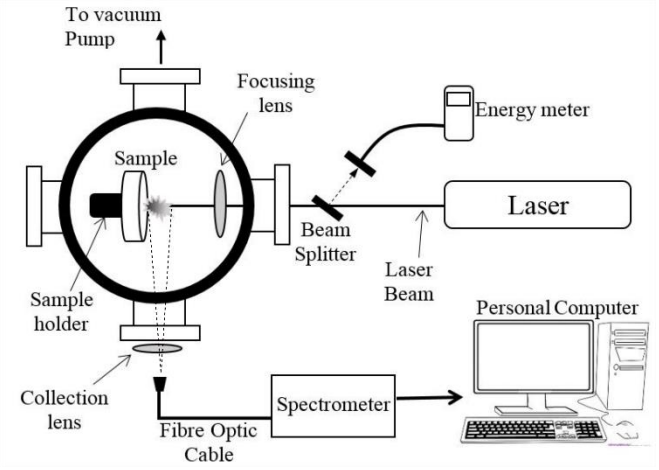

Fig. 5.1 Schematic illustration of a typical laboratory LIBS setup [2]

The alignment of FOC is crucial; its distance and orientation to the plasma plume is optimised for the best signal and kept constant for the whole set of measurements. As the distance between FOC and plasma varies, radiation intensity collected by the FOC also varies. Therefore, the distance of the FOC from the target (plasma plume) can be optimised by observing the intensity of a spectral line of interest. In Fig. 5.2(a) the intensity of Mg II (279.55 nm) line is plotted against the distance between FOC and target sample. With increasing distance, the emission intensity decreases exponentially. Here, the optimum distance is considered as the one at which maximum intensity of the Mg II line is obtained without saturating the detector response.

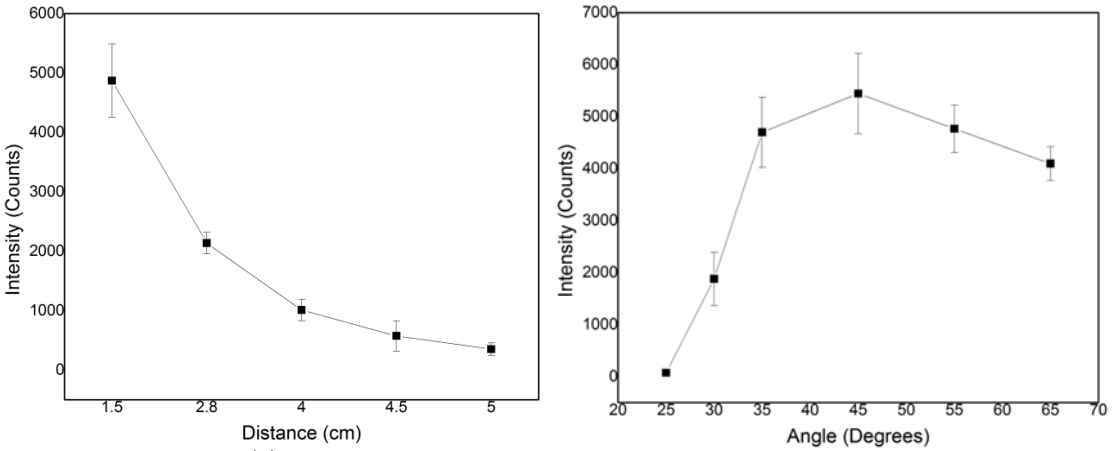

Fig. 5.2 Intensity variation of Mg II line (279.55 nm) with distance and orientation of FOC with reference to the target

At the optimised distance from the ablation spot (target), the orientation angle of the FOC is optimised in the range 25-65° with respect to the sample surface. An optimised angle is considered to be the one at which the maximum intensity of Mg II (279.55 nm) line is recorded. From Fig. 2(b), the angle 45° w.r.to the sample surface is the optimised angle since the intensity of the emission line clearly decreases before and after 45° because of reduction in the radiation collection.

5.3 Plasma Characterizations

5.3.1 Spectral Emissions and Self Absorption

Laser-induced plasma is transient in nature. It evolves and decays during its very short lifetime. After ignition, the excited plume expands and then decays within a few 10s of microseconds at atmospheric pressure. Plasma emissions vary during this time, and it is very important to know which time window, i.e. gate delay, would be the best for intended measurements.

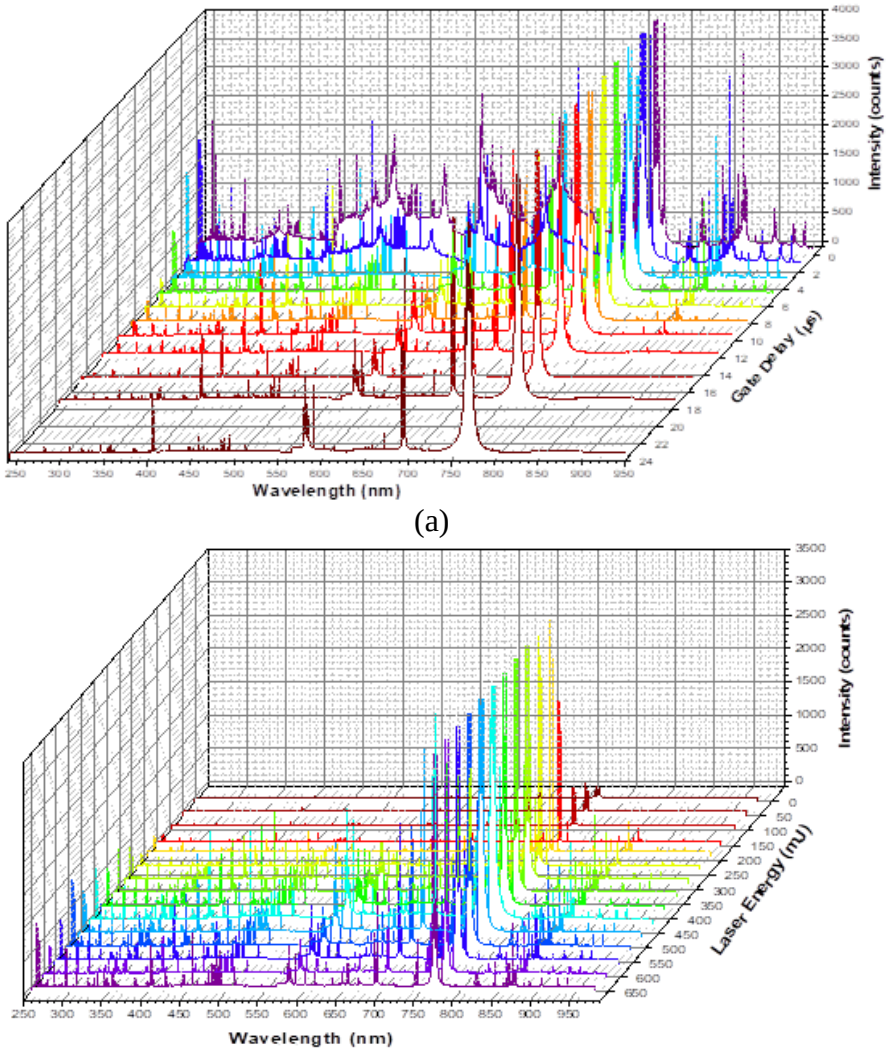

Fig. 5.3 Variation in spectral intensity with change in (a) gate-delay of measurements, and (b) laser energy [3]

Fig. 5.3 shows variation in spectral intensity with change in gate delay from 0 to 23.75 μs and change in laser energy from ~5 to 650 mJ. After plasma ignition, both continuum (resulting from free-free and free-bound interactions) and line emissions (resulting from electronic transitions) are prominent. During the first 3 μs, continuum emissions are considerably strong which are deemed undesired in common circumstances.

Line emissions are the most important spectral features in the LIBS spectrum which dominate the spectrum only after a certain delay after the plasma ignition. The background signal in Fig. 5.3(a) diminishes with the increase in gate delay. As the plasma expands, a reduction in continuum emission occurs because of the decrease in electron-ion recombination and bremsstrahlung processes. As the plasma decays, atomic spectral lines and, later, molecular lines/bands can be observed due recombination of electrons and ions into atoms and molecules.

Understanding the change in spectral intensity with change in laser energy is straight forward. It implies that the higher energy laser pulse energises plasma more than a weaker laser pulse and results in a higher degree of excitation and hence intense radiations, as seen in Fig. 5.3(b).

5.3.2 Self-Absorption Measurements in Spectral Lines

Resonant lines, i.e. spectral lines involving ground state, are most prone to self-absorption (SA). If resonant lines are optically thin (free of SA), it is safe to rule out SA in non-resonant lines. Therefore, we considered emission lines Al I 308.2 nm and 309.3 nm for investigating SA which include ground energy level ($3s^2 3p$) in the radiative transition.

SA coefficient is used as an indicator of the self-absorption. We utilised one of the simplest ways of determining SA coefficient with the help of the following expression.

$$SA = \left(\frac{\Delta\lambda}{2\omega_s} \frac{1}{N_e} \right)^{\frac{1}{\alpha}} \tag{5.1}$$

Where $\Delta\lambda$, ω_s, α and N_e are is the FWHM of the spectral line, Stark broadening parameter, absorption coefficient and electron density respectively. Details about it can be found in [3]. The closer the SA coefficient is to unity, the smaller is the self-absorption.

The laser energy increased from 5 to 650 mJ has caused the SA coefficient to increase from 0.05 to 0.9 (Fig. 5.4(a)). As the atoms decay to the ground state, the emitted photons will have a high probability of being absorbed on their way out from the plasma. It is found that with an increase in the laser energy the influence of self-absorption on the Al I 308.2 nm and Al I 309.3 nm continues to decrease and at 650 mJ of laser energy SA coefficient for Al I 308.2 is close to unity which refers to negligible self-absorption. As higher laser energy irradiated onto the sample's surface, more intense plasma radiation is observed because of the higher degree of dissociation and excitation of the species. Self-absorption often occurs due to the excitation gradient from the core to the peripheral region of the plasma. Hence, when the de-excitation of atoms occurs in the central/core region of the plasma to produce resonant spectral lines, the photons get absorbed by the atoms/ions which are in the ground state in the peripheral region of the plasma.

As depicted in Fig. 5.4(b), the SA coefficient drops from 0.9 to 0.1 for an increase in the gate delay from 0 to 20 μs. At the initial stage of plasma generation, the

SA coefficient is near to unity, so, the plasma can be considered optically thin for the emission lines. This is because of the high degree of excitation of plasma species. However, as the plasma evolves, the SA starts to pronounce and gets stronger at larger gate delays. The decreasing trend in SA coefficient can also be explained based on its dependence on plasma temperature variation, the equilibrium between ions and atoms, and plasma expansion. As the gate delay increases, the plasma temperature and density are decreased because of plasma expansion, thereby increasing the possibility of self-absorption. Therefore, one should capture emission of plasma at early delay settings if optically thin resonant lines are the utmost priority.

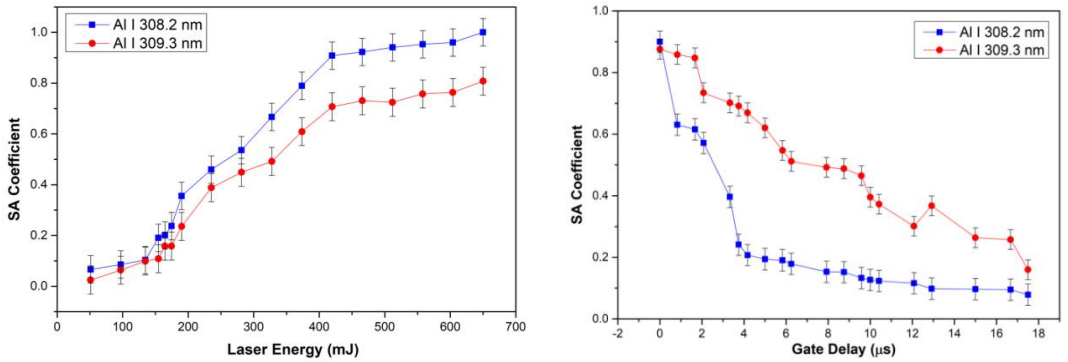

Fig. 5.4 SA in response to the (a) Laser Energy and (b) Gate Delay for Aluminium spectral lines Al I 308.2nm and 309.3 nm. [3]

5.4 Application of LIBS

5.4.1 Determination of lead in Plant leaves and Soil Samples

Organic samples are complex materials, and LIBS is sensitive to the matrix. Therefore, matrix-matched calibration samples are a better choice to minimise sample-induced effects in quantitative measurements. Laboratory prepared calibration samples of known composition (see Table 5.1 in [4]) were used to obtain calibration curves to determine Pb in *Phaleria Macrocarpa* leaves and soil samples. Representative spectra of *Phaleria Macrocarpa* (locally known as *Mahkota Dewa*) leaves, and *soil* are presented in Fig. 5.5. The intensities of lead lines are plotted against Pb concentration in calibration samples. The Pb I 363.95 nm was chosen for having the most linear correlation with Pb concentration. Analytical measurements at 500 mbar (optimised ambient for best signal-to-background ratio) of air are shown as calibration curves in Fig. 5.6. Each point in the calibration plot is an average of at least fifteen measurements. Error bars represent the standard deviation in the measurements. Black squares symbolise calibration samples while red squares represent prediction (unknown concentration) samples. Prediction samples were not utilized in the linear regression. The calibration curves are linear, with correlation coefficients better than 0.98, as shown in Figs. 5.6(a) and (b) for *Phaleria Macrocarpa* and *soil*, respectively.

The slope of a calibration curve signifies the sensitivity of the measurement. The higher the slope, the better is the sensitivity.

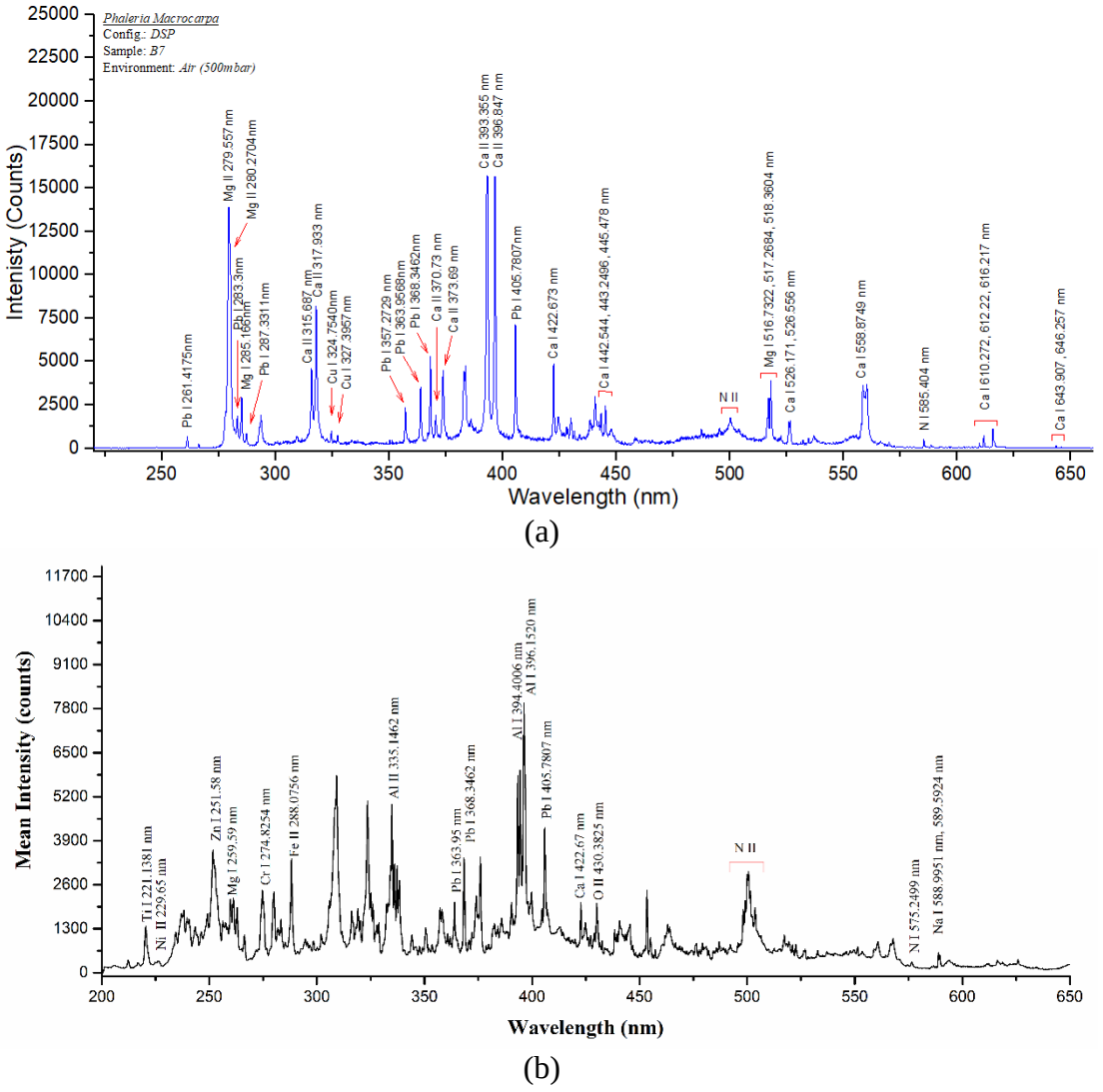

Fig. 5.5 LIBS spectrum of (a) *Phaleria Macrocarpa* and (b) Soil using 100 mJ of laser energy in air environment [4]

To evaluate the performance, root mean square error of prediction (RMSEP) and maximum relative error (MRE) were calculated using Eqs. 5.2 and 5.3 respectively and the values are listed in Table 5.1.

$$RMSEP = \sqrt{\sum_{s=1}^{N} \frac{\left(C_{pre,s} - C_{nom,s}\right)^2}{N}} \tag{5.2}$$

$$MRE = \max\left(\left|\frac{C_{pre,s} - C_{nom,s}}{C_{nom,s}}\right|_{s=1}^{N} \times 100\%\right) \quad (5.3)$$

Here $C_{pre,s}$ and $C_{nom,s}$ are the predicted, and nominal concentrations of a sample s and N is the total number of samples used in the estimation. The limit of detection is determined as $3.3*\sigma/m$, where σ is the standard deviation of blank measurements and m is slope of the calibration curve. Lower error, a better limit of detection, and good precision are obtained for the analysis of soil. However, smaller values of maximum relative error (MRE) were obtained for the leaf samples. The varying concentrations in soil and leaves affect the accuracy and precision of the measurement. Another important factor is the sample heterogeneity that can influence the precision of the measurements.

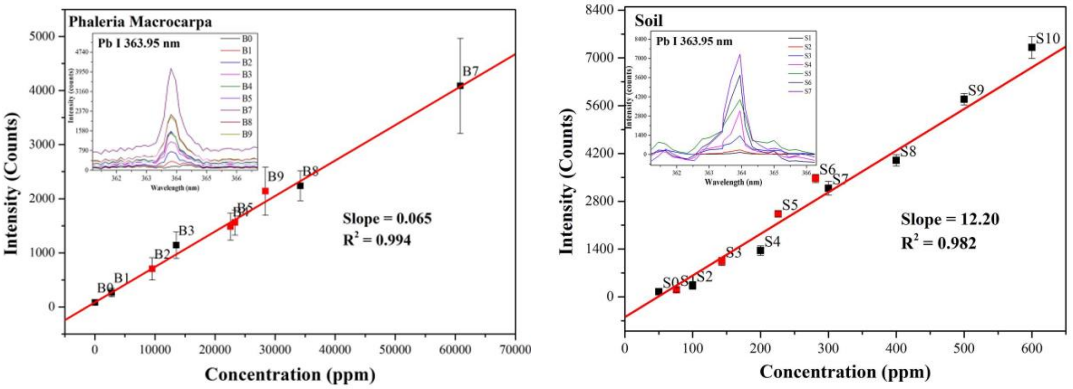

MRE: 10.7% (a) MRE: 18.6% (b)

Fig. 5.6 Calibration Curves for estimation of Pb estimation in leaves and soil samples [4]

Table 5.1, Analytical figures of merit for Phaleria Macrocarpa and soil by LIBS [4]

Samples	RMSEP (ppm)	MRE (%)	RSD (%)	LOD (ppm)
Leaves	1673.64	10.69	14.99	1017.71
Soil	29.16	18.59	3.42	15.96

5.4.2 Determining Ca/P Ratio in Hydroxyapatite

Hydroxyapatite (HA) is an important biomaterial for making bone cement which is used for repairing cracked bones. The value Ca/P ratio is an indicator of the composition of HA suggested for bone cement. LIBS can be a rapid and real-time

analytical technique to monitor the Ca/P ratio in HA in the procedure of bone cement preparation, as demonstrated below with preliminary investigations. We studied the Ca/P ratio in natural HA, extracted from Lamb, Fish and Bovine bones [5][6] and the synthetic HA, prepared in laboratory [7] using LIBS.

LIBS spectrum of HA is presented in Fig. 5.7. Lines of major constituents of HA, i.e. Ca, P, K and Br were identified in the spectrum using NIST atomic spectra database. The intensity of spectral lines in emission spectra is indicative of elemental concentration. However, different spectral lines of the same element do not respond equally to a similar change in the element's concentration. Ca I 610.27 nm and P I 550.72 nm were selected to calculate Ca/P ratio in the sample as it gave closest to the stoichiometric values (also verified by EDX). A comparison of Ca/P ratios obtained from LIBS and EDX is given in Table 5.2.

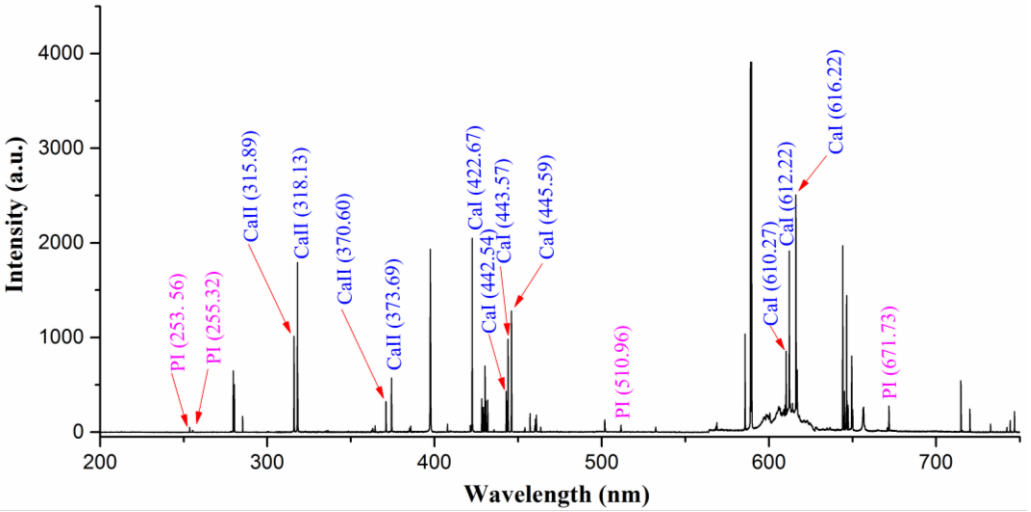

Fig. 5.7 LIBS spectrum of HA extracted from bovine bone [5]

The average Ca/P ratio obtained from the LIBS analysis were compared with EDX measurements. Figures 8a & 8b show the graph Ca/P ratio for both techniques for each natural HA samples and synthetic HA samples, respectively. These values are within the accepted range (1.86-1.97) for natural HA and close to stoichiometric ratios in synthetic HA.

It is evident from Fig. 5.8 that the values of Ca/P ratios obtained for different samples obtained with LIBS are fairly close to the values obtained from EDX technique which is an established technique for determining the elemental composition of a material. Therefore, it can be concluded that LIBS can be potentially used reliably for such type of investigations with added benefits of rapid, real-time and non-destructive analysis.

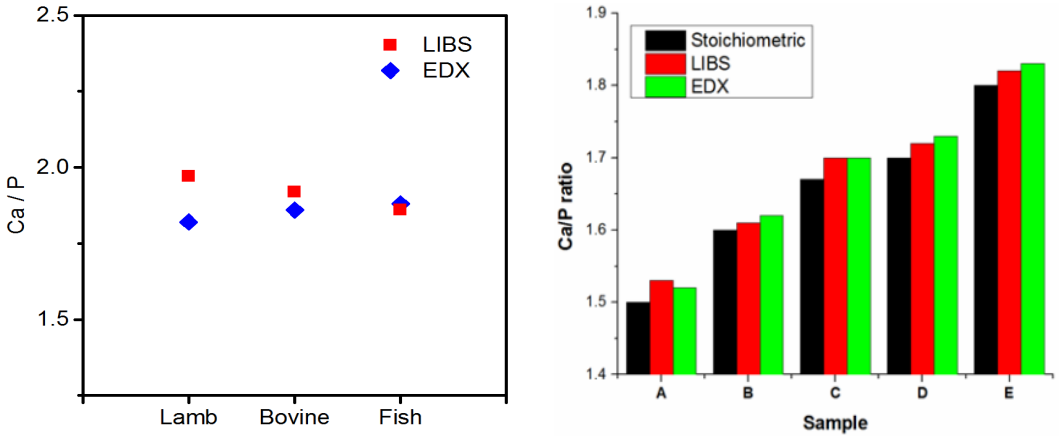

Fig. 5.8 Comparison between Ca/P ratios determined from EDX and LIBS [6], [7]

Table 5.2 Comparison of Ca/P ratio measurements with EDX and LIBS in synthetic HA samples

Sample	Stoichiometric Ca/P ratio	Ca/P ratio by EDX	Ca/P ratio by LIBS
A	1.50	1.52	1.53
B	1.60	1.62	1.61
C	1.67	1.70	1.70
D	1.70	1.73	1.72
E	1.80	1.83	1.82

5.4.3 Classification of Metallic Samples

Emission spectra are the optical signatures of material, and therefore, ideally, one should be able to identify and discriminate a material using its LIBS spectrum. It is easier when samples are far different in composition, i.e. metals & alloys and becomes difficult when they have nearly the same composition, e.g. biological samples. When we cannot differentiate with the naked eye, we can make use of discrimination tools. Principal Component Analysis (PCA) has proved very useful in this regard. PCA performs dimensional reduction on the data and generates PCs in descending order of variance in that data. It makes it easy to classify the data using the top few PCs, generally, PC1, PC2 and PC3.

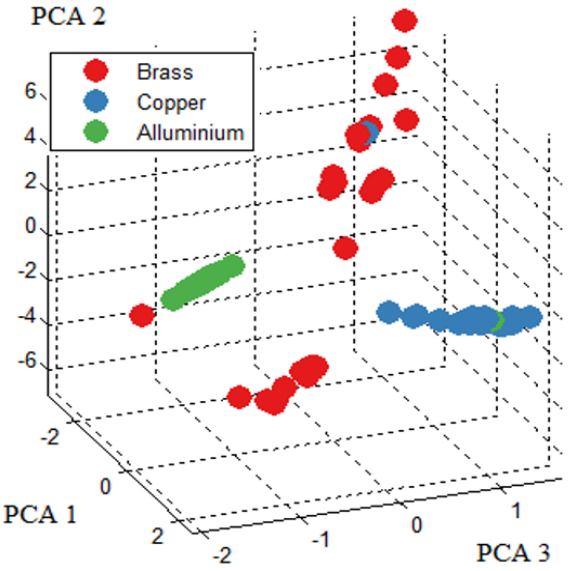

Fig. 5.9 Classification of (a) meat samples and (b) metallic samples using PCA and LIBS

Fig. 5.9 shows the classification of Al, Brass and Zn using PCA on LIBS data comprising of 75 spectra (25 per sample). PCA was performed on the spectral data to generate PCs. The principal component scatter plot of PC1, PC2 and PC3 (Fig. 5.9) shows the difference between the three samples. Clear clustering shows three distinctive groups of data. Here, Al, Brass and Cu of different purifications are grouped into their family of the major element. It shows the possibility of discrimination of materials based on their LIBS spectra and the effectiveness of PCA technique in this application.

REFERENCES

[1] Z. Haider, Y. Bin Munajat, R. Kamarulzaman, and N. Shahami. (2015) Comparison of single pulse and double simultaneous pulse laser induced breakdown spectroscopy. *Anal. Lett.* 48, 2, 308–317.

[2] K. Chaudhary, S. Z. H. Rizvi, and J. Ali. (2016) Laser-Induced Plasma and its Applications. in *Plasma Science and Technology - Progess in Physical States and Chemical Reactions*, T. Mieno, Ed. Rijeka: InTech, 259–291.

[3] N. M. Sabri, Z. Haider, K. Tufail, F. D. Ismail, and J. Ali. (2018) Spectroscopic diagnostics of laser induced plasma and self-absorption effects in Al lines. *Phys. Plasmas*. 25, 7, 073303.

[4] Z. Haider *et al.* (2016) Plasma diagnostics and determination of lead in soil and phaleria macrocarpa leaves by ungated laser induced breakdown spectroscopy. *Anal. Lett.* 49, 6, 808–817.

[5] U. Tariq, Z. Haider, R. Hussain, K. Tufail, and J. Ali. (2017) LIBS analysis of hydroxyapatite extracted from bovine bone for Ca/P ratio measurements. *AIP Conference Proceedings*. 030027.

[6] E. Mazalan, K. Chaudhary, Z. Haider, S. F. Abd Hadi, and J. Ali. (2018) Determination of calcium to phosphate elemental ratio in natural hydroxypatite using LIBS. *J. Phys. Conf. Ser.* 1027, 1, 012013.

[7] U. Tariq, Z. Haider, K. Chaudhary, R. Hussain, and J. Ali. (2018) Calcium to phosphate ratio measurements in calcium phosphates using LIBS. *Journal of Physics: Conference Series*. 1027, 1.